Fossil shell emission in dying radio loud AGNs

M. Kino[1,⋆], **H. Ito**[2], **N. Kawakatu**[3], **M. Orienti**[4], **H. Nagai**[5], **K. Wajima**[1], and **R. Itoh**[6]

[1] KASI, 776 Daedeokdae-ro, Yuseong-gu, Daejeon 305-348, Republic of Korea
[2] Astrophysical Big Bang Laboratory, RIKEN, Saitama 351-0198, Japan
[3] National Institute of Technology, Kure College, 2-2-11 Agaminami, Kure, Hiroshima, 737-8506, Japan
[4] INAF - Istituto di Radioastronomia, via Gobetti 101, 40129 Bologna, Italy
[5] National Astronomical Observatory of Japan, 2-21-1 Osawa, Mitaka, Tokyo, 181-8588, Japan
[6] Hiroshima University, Higashi-Hiroshima, Hiroshima 739-8526, Japan

Received 2015 June 30, accepted 2015
Published online 2015

Key words galaxies: active, galaxies: jets, gamma rays: galaxies, radiation mechanisms: non-thermal, radio continuum: galaxies

We investigate shell emission associated with dying radio loud AGNs. First, based on our recent work by Ito et al. (2015), we describe the dynamical and spectral evolutions of shells after stopping the jet energy injection. We find that the shell emission overwhelms that of the radio lobes soon after stopping the jet energy injection because fresh electrons are continuously supplied into the shell via the forward shock while the radio lobes rapidly fade out without jet energy injection. We find that such fossil shells can be a new class of target sources for SKA telescope. Next, we apply the model to the nearby radio source 3C84. Then, we find that the fossil shell emission in 3C84 is less luminous in radio band while it is bright in TeV γ ray band and it can be detectable by CTA.

1 Introduction

Radio-loud active galactic nuclei (AGNs) are one of the most powerful objects in the universe. According to the standard picture of jets in AGNs, jets are enveloped in a cocoon consisting of shocked jet material and the cocoon is surrounded by shocked interstellar medium region (e.g., Begelman et al. 1984). The shocked interstellar medium region (hereafter we refer to as the shell) is identical to the forward shocked region and it is a fundamental ingredient in the overall AGN jet system. Physical properties of shells, however, have not been well understood since they are not bright and remain undetected (but see Croston et al. (2009) for X-ray emission from shell in Centaurus A). In the radio band, shells are radio quiet (Carilli et al. 1988) and their emission is fully overwhelmed by the radio bubbles (radio lobes). The existence of the radio quiet shell (bow shock) is only identified as the discontinuity of the rotation measure in the radio lobes of Cygnus A (Carilli et al. 1988).

In terms of observing shells, bright radio lobes prevent their detection. Then, we come up with a question of "what happens when jet energy injection stops?" Motivated by this question, we recently explore the emission from radio sources in which jet activity has ceased at early stage of their evolution in Ito et al. (2015) (hereafter I15). In particular, we focus on the evolution of the relative contribution of the lobe and shell emission. In this work, we will show that the shell will be dominant at most of the frequencies from radio up to TeV γ-ray soon after the jet has switched off.

The layout of this paper is as follows. In §2, we present the review of the model following the formulation shown in I15. In §3, we apply the model to a typical dying radio-loud AGN at $z = 1$. We will show that their fossil shell emission can be probed with the Square Kilometer Array (SKA). In §4, we apply the model to the dying radio lobes observed in 3C84. Summary and discussions are presented in §5.

2 Basic Model

Since the details of the model of pressure-driven expanding jet-remnant system have been already well explained in Ito et al. (2011) and I15 and references therein, here we briefly summarize the main ingredients.

2.1 Dynamics

Fig. 1 presents a general picture of a jet and external medium interaction and we adopt the well established expanding spherical bubble model (I15 and reference therein). The shell width at the bubble radius ($R(t)$) at the time t is denoted by δR. The mass density of the ambient matter at $R(t)$ is defined as $\rho(R) = \rho_0 R$ where R_0 is the reference radius, δR satisfies the relation

$$\delta R = (\hat{\gamma}_{\rm ext} - 1)[(\hat{\gamma}_{\rm ext} + 1)(3 - \alpha)]^{-1} R, \quad (1)$$

where $\hat{\gamma}_{\rm ext}$ and α are, respectively, the specific heat ratio of the external medium and the index of external ambient

⋆ Corresponding author: e-mail: kino@kasi.re.kr

matter density distribution defined as $\rho \propto R^{-\alpha}$. We assume that the kinetic power of the jet ($L_{\rm j}$) is constant in time. The jet kinetic energy is dissipated and deposited as the internal energy of the cocoon and shell. [1]

In this work, we consider two phases depending on the source age (t):

– (i) the phase in which the jet energy injection into the cocoon continues ($t < t_{\rm j}$)
– (ii) the phase in which the jet energy injection into the cocoon stops ($t > t_{\rm j}$)

where $t_{\rm j}$ denotes the duration of the jet injection.

As for the early phase with jet energy injection into the cocoon, the radius of the cocoon is given by

$$R(t) = C R_0^{\frac{\alpha}{\alpha-5}} \left(\frac{L_j}{\rho_0}\right)^{\frac{1}{5-\alpha}} t^{\frac{3}{5-\alpha}} \quad (t < t_{\rm j}) \tag{2}$$

where C and R_0 are the numerical coefficient and the reference size of the cocoon, respectively. Note that $L_{\rm j}/\rho_0$ is the key quantity which controls the dynamical evolution of AGN jet system (e.g., Kawakatu et al. 2009).

After the energy injection from the jet ceases, the cocoon will rapidly lose its energy due to adiabatic expansion and most of its energy is transferred into the shell within a dynamical timescale. Hence, after the transition time, the cocoon pressure becomes dynamically unimportant, and the energy of the shell becomes dominant. Therefore, in the late phase, expansion of the bow shock asymptotically would follow the Sedov-Taylor expansion. Therefore we set

$$\dot{R}(t) \propto t^{-(3-\alpha)/(5-\alpha)} \quad (t > t_{\rm j}). \tag{3}$$

In this phase, the adiabatic relation $P_c V_c^{\hat{\gamma}} = {\rm const.}$ should hold. Then, we can approximately describe the late phase as follows:

$$R(t) = R(t_{\rm j}) \left[\frac{P(t_{\rm j})}{P(t)}\right]^{1/3\hat{\gamma}} \quad (t > t_{\rm j}). \tag{4}$$

We set $\hat{\gamma}_{\rm ext} = 5/3$ and $\hat{\gamma} = 4/3$ for the shock jump condition between the shell and external medium (I15).

2.2 Non-thermal emission

Since the details of the treatment of non-thermal emissions have been already explained in Kino et al. (2013) (hereafter K13) and I15, we briefly show the basic treatment of photon and electron distributions in shells and lobes. We solve the set of kinetic equations describing the electron and photon energy distributions. First, as for the external photon field against inverse Compton (IC) process, (1) UV photons from a standard accretion disk, (2) IR photons from a dust torus, (3) synchrotron photons from the radio lobes, and (4) synchrotron photons from the shell are included. Second,

[1] The dense thermal gas surrounding 3C84 has been discovered by O'Dea et al. (1984). However, in this work, we focus on the diffuse ambient matter and neglect the dense thermal (torus) component merely for simplicity. The case of shocks in the dense thermal gas will be presented in a forthcoming paper (Kino et al. in prep).

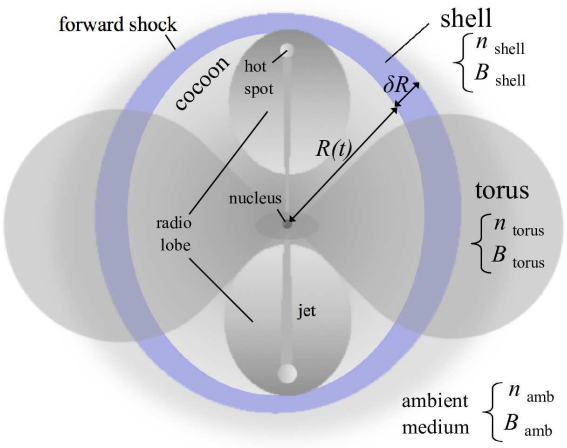

Fig. 1 Schematic picture of the jet and external medium interaction in face-on view. The kinetic energy of the jets is dissipated via the termination shock at the hot spots and deposited into the cocoon with its radius R and the shell with its width δR. The cocoon is inflated by its internal energy. The cocoon drives the forward shock propagating in the external medium with its density and magnetic field strength $n_{\rm ext}$ and $B_{\rm ext}$. The forward shocked region is identical to the shell.

we include the effect of absorption via $\gamma\gamma$ interaction. VHE photons suffer from absorption via interaction with various soft photons. Here, we include the $\gamma\gamma$ absorption due to both source-intrinsic and EBL (Extragalactic Background Light) photon fields. The absorption opacity with respect to the intrinsic photons can be calculated by summing up all of the photons from (1) the shell, (2) the radio lobes, (3) the dusty torus, and (4) the accretion disk and we multiply the $\gamma\gamma$ absorption factor of $\exp(-\tau_{\gamma\gamma})$ with the unabsorbed flux where $\tau_{\gamma\gamma}$ is the optical depth for the $\gamma\gamma$ absorption. For simplicity, we deal with the absorption effect at the first order and we neglect cascading effect. With regard to the opacity for $\gamma\gamma$ interaction between EBL and TeV γ photons, we adopt the standard model of Franceschini et al. (2008).

3 Application to high-z dying radio sources

3.1 Setting

Here we demonstrate the time evolutions of the energy distribution of non-thermal electrons and the resulting emission. As a fiducial case we focus on sources with jet power of $L_{\rm j} = 1 \times 10^{45}$ erg s^{-1} at $z = 1$. We set the duration of energy injection as $t_{\rm j} = 10^5$ yr. The chosen value of the age is around the upper end of the estimated age of the compact radio source with an overall linear size of 5 kpc (e.g., Murgia et al. 1999).

Regarding the IC scattering, full Klein-Nishina (KN) cross section is taken into account. As a source of seed photons, we consider UV emission from the accretion disc, IR emission from the dusty torus, stellar emission in NIR

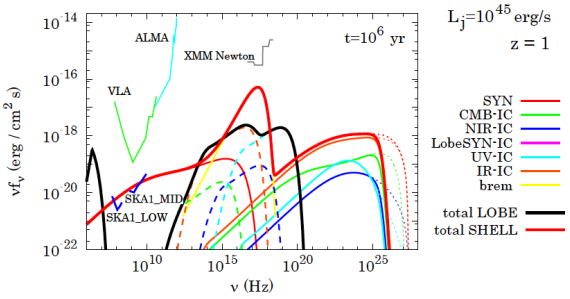

Fig. 2 Broadband spectrum of a dying radio source with a jet power of $L_{\rm j} = 1 \times 10^{45}$ erg s^{-1} located at z = 1. The figure is adopted from I15. The source age in this case is 10^6 yr and the jet injection has been stopped since $t_{\rm j} = 10^5$ yr. The thick lines show the total flux from the shell and lobe. The various thin dashed and thin solid lines show the contributions to the total emission produced in the lobe and shell, respectively. (A color version of this figure is available in the online journal.) The shell emission can be detected by SKA. The SKA sensitivity curves correspond to 3 sigma detection limit with 10 hours of integration time (Prandoni & Seymour 2015).

from the host galaxy, synchrotron emission from the radio lobe and cosmic microwave background (CMB). We constructed the model of the spectra of the photons from the disc, torus and host galaxy with a black-body spectra. As for the luminosities of the emissions, we adopt $L_{\rm UV} = L_{\rm IR} = 1 \times 10^{45}$ erg s^{-1} for the disc and torus emission (e.g., Elvis et al. 1994; Jiang et al. 2006), and $L_{\rm IR} = 1 \times 10^{44}$ erg s^{-1} for the host galaxy emission (e.g., de Ruiter et al. 2005).

3.2 Results: Long-lived shell emission in high-z radio-loud sources as a new target for SKA

In Fig. 2, we show the resultant spectra from the radio lobe and shell after the jet injection was stopped. We examine the typical case with the conservative jet power $L_{\rm j} = 1 \times 10^{45}$ erg s^{-1} at $z = 1$, and the electron acceleration efficiency in the shell $\epsilon_{e,\rm shell} = 0.01$. We found that the shell emission overwhelms that of the radio lobes soon after stopping the jet energy injection because fresh electrons are continuously supplied into the shell via the forward shock while the radio lobes rapidly fade out.

Regarding the detectability of the shell emission, SKA telescope is capable of detecting the emission. The detection is marginal for SKA phase 1. Since these values inevitably have dispersion from source to source, we expect a certain fraction of sources to be well above the detection limit. Moreover, in the phase 2 (SKA2), the sensitivity is expected to improve by an order of magnitude. Hence, SKA will be a powerful tool to reveal the population of dead radio sources which are dominated by the shell emission.

4 Application to 3C84

The compact radio source 3C84, also known as the Seyfert galaxy NGC1275 (at the redshift $z = 0.0176$) is one of the ideal target for this study.

In Fig. 3, we show the two epoch comparison of VLBA images obtained at 15 GHz obtained in 1994 and 2010. From this, we can clearly see that the pair of outer radio lobes on ~ 10 mas scale is fading out due to the lack of jet energy injection. Hereafter, we examine the shell emission associated with this fading radio lobes.

4.1 Setting

Number densities of surrounding medium are important quantities but they have some degree of uncertainties. Taylor et al. (2006) estimated the number density by using deep Chandra observation (Fabian et al. 2006). Within the central 0.8 kpc, the density profile is severely affected by the nucleus. So, they estimated an average central density over the inner 2 kpc to be $n_{\rm amb} \sim 0.3$ cm^{-3}. Regarding the upper limit on the number density, recently Fujita et al. (2014) obtained $n_{\rm amb} \sim 10$ cm^{-3} for the inner part of Perseus cluster by taking the following two assumptions: (1) hot gas outside the Bondi radius is in nearly a hydrostatic equilibrium in a gravitational potential, and (2) the gas temperature near the galaxy centre is close to the virial temperature of the galaxy. In this work, we adopt $n_{\rm amb} = 1$ cm^{-3} which is in between these values.

Energy densities of surrounding photon fields are also important quantities. They are seed photons for IC scattering. As for UV from the accretion disc, we set

$$L_{UV} = 5 \times 10^{42} \ {\rm erg \ s^{-1}}, \quad (5)$$

based on the observation of Kanata telescope (see Appendix) and we conservatively include the safety factor $1/2$ to mimic a possible contamination of extended sources. The accretion flow can be safely regarded as a point source. Regarding IR dust, we set $L_{\rm IR} = L_{\rm UV}/2$ based on Calderone et al. (2012). Note that IR torus is supposed to be extended up to 10 pc scale in order to produce the free-free absorption observed at the northern radio lobe (Walker et al. 2000). Fluxes of synchrotron emission from radio lobes are adopted from the actual observational data. As for the mini radio lobes at ~ 3 mas scale (Nagai et al. 2010; Nagai et al. 2012; Suzuki et al. 2012), we set

$$L_{\rm mini-lobe} \approx 1 \times 10^{43} \ {\rm erg \ s^{-1}} \quad (6)$$

at $\sim$ 200 GHz based on the recent flux level of 3C84 in SMA calibrator list.

Let us discuss the total jet power in 3C84. The observed luminosity at each energy band is of order of $\sim 10^{43}$ erg s^{-1} from radio to GeV γ-ray band (Abdo et al. 2009). Therefore, the bolometric luminosity is estimated as close to $\sim 10^{44}$ erg s^{-1}. Hence, for example, a typical 10 % radiative efficiency of non thermal electrons results in the electron kinetic power of order of close to $\sim 10^{45}$ erg s^{-1}.

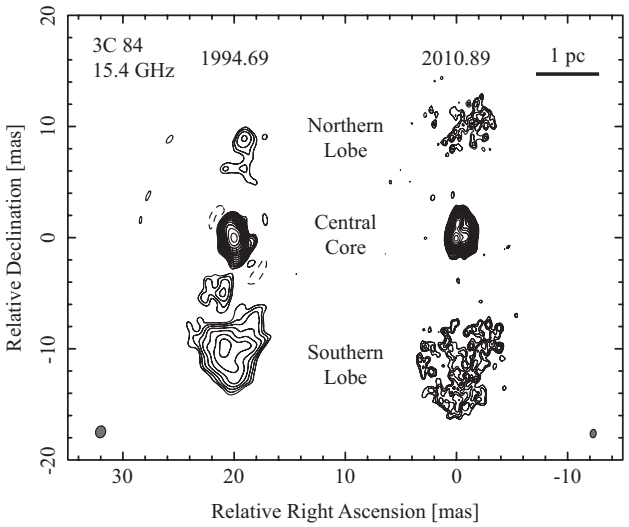

Fig. 3 VLBA images of 3C 84 obtained at 15.4 GHz. Images refer to observations performed on 1994 September 10 (left) and 2010 November 20 (right). The lowest contour is three times the off-source rms noise (one σ), and the contour levels are -3σ, $3\sigma \times (\sqrt{2})^n$ (n = 0, 1, 2, ...). The peak intensity is 5.86 Jy beam^{-1} (left) and 5.54 Jy beam^{-1} (right). The restoring beam is indicated in the bottom left/right corner of the left/right images. The total flux density of northern and southern lobes are 0.8 Jy and 6.7 Jy in 1994, while they decrease to 0.5 Jy and 1.4 Jy in 2010, respectively.

Table 1 Parameters of radio lobes and shell in 3C84

$L_{\rm j}$ (erg s^{-1})	$B_{\rm shell}$ (mG)	$n_{\rm amb}$ (cm^{-3})	$\epsilon_{e,\rm shell}$ –	$\epsilon_{e,\rm lobe}$ –
3×10^{45}	0.2	1	0.1	0.1

Proton component is also supposed to contribute to the total jet power. Based on this order estimation, we set $L_{\rm j} = 3 \times 10^{45}$ erg s^{-1} in the present work.

4.2 Results: Long-lived shell emission in 3C84 as a new target of CTA

In Fig. 4, we show a prediction of the broadband spectrum from the fossil shell in 3C84 10 years after the jet cessation. The significant difference between this case and the above section is the distance of the sources from the Earth. Since the redshift of 3C84 is sufficiently low, $\gamma\gamma$ absorption with the EBL is less effective. Therefore, it can be a new TeV gamma-ray emitter candidate. We find that the IC emission can be detectable by the Cherenkov Telescope Array (CTA) in this case. We also find that the synchrotron photons from the radio lobes are the dominant seed photons for the IC scattering in 3C84. The detailed comparison of the contribution from mini-radio lobes will be presented in a forthcoming paper (Kino et al. in preparation).

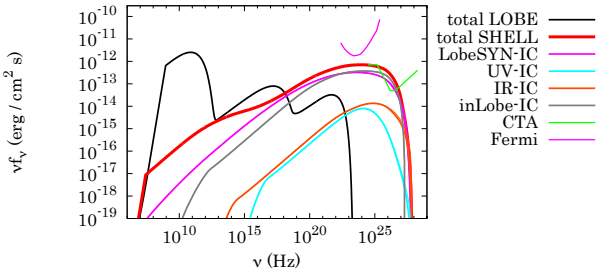

Fig. 4 Fossil shell spectrum 10 years after the jet cessation in 3C84 (the thick curve peaked at gamma-ray energy band). The shell spectrum is IC dominated. There are four components of the seed photons for IC scattering; i.e., synchrotron photons from outer and inner radio lobes, UV from the accretion disk, and IR from the torus. Among them, synchrotron photons from outer and inner radio lobes are dominant (A color version of this figure is available in the online journal.)

5 Summary

In the present work we studied a possible fossil shell emissions associated with dying radio loud AGNs. Below, we summarize the main results.

- We reviewed our recent work presented in I15. We have examined the dynamical and spectral evolution of fossil shells which are identical to the forward shocks propagating in the external medium. We find that the shell emission overwhelms that of the radio lobes soon after stopping the jet energy injection because fresh electrons are continuously supplied into the shell via the forward shock while the radio lobes rapidly fade out.
- Fossil shell emission in high-z dying radio sources is presented. We examine the typical case with the conservative jet power $L_{\rm j} = 1 \times 10^{45}$ erg s^{-1} at $z = 1$, and electron acceleration efficiency in the shell $\epsilon_{e,\rm shell} = 0.01$. Regarding future facilities, SKA telescope is capable of detecting the emission in the radio band. The detection is marginal for SKA phase 1.
- Fossil shell emission in 3C84 is investigated by applying I15 model. Since 3C84 is a low redshift source, $\gamma\gamma$ absorption is less effective. We examine the broadband spectrum from the fossil shell in 3C84 10 years after the jet cessation with the jet power $L_{\rm j} = 3 \times 10^{45}$ erg s^{-1}, and relatively large electron acceleration efficiency in the shell $\epsilon_{e,\rm shell} = 0.1$. We find that the IC emission can be detectable by CTA.

Acknowledgements. The research leading to these results has received funding from the European Commission Seventh Framework Programme (FP/2007-2013) under grant agreement No 283393

(RadioNet3). Part of this work was done with the contribution of the Italian Ministry of Foreign Affairs and University and Research for the collaboration project between Italy and Japan. This research has made use of data from the MOJAVE database that is maintained by the MOJAVE team (Lister et al., 2009) .

References

Abdo, A. A., Ackermann, M., Ajello, M., et al. 2009, ApJ , 699, 31
Begelman, M. C., Blandford, R. D., & Rees, M. J. 1984, Reviews of Modern Physics, 56, 255
Calderone, G., Sbarrato, T., & Ghisellini, G. 2012, MNRAS , 425, L41
Carilli, C. L., Perley, R. A., & Dreher, J. H. 1988, ApJ , 334, L73
Croston, J. H., Kraft, R. P., Hardcastle, M. J., et al. 2009, MNRAS , 395, 1999
de Ruiter, H. R., Parma, P., Capetti, A., et al. 2005, A&A, 439, 487
Elvis, M., Wilkes, B. J., McDowell, J. C., et al. 1994, ApJS , 95, 1
Fabian, A. C., Sanders, J. S., Taylor, G. B., et al. 2006, MNRAS , 366, 417
Franceschini, A., Rodighiero, G., & Vaccari, M. 2008, A&A, 487, 837
Fujita, Y., Kawakatu, N., & Shlosman, I. 2014, arXiv:1406.6366
Greene, J. E., & Ho, L. C. 2005, ApJ , 630, 122
Ho, L. C., Filippenko, A. V., Sargent, W. L. W., & Peng, C. Y. 1997, ApJS , 112, 391
Ito, H., Kino, M., Kawakatu, N., & Yamada, S. 2011, ApJ , 730, 120
Ito, H., Kino, M., Kawakatu, N., & Orienti, M. 2015, ApJ , in press (I15)
Jiang, L., Fan, X., Hines, D. C., et al. 2006, AJ , 132, 2127
Kawabata, K. S., Nagae, O., Chiyonobu, S., et al. 2008, SPIE, 7014, 70144L
Kawakatu, N., Kino, M., & Nagai, H. 2009, ApJ , 697, L173
Kino, M., Ito, H., Kawakatu, N., & Orienti, M. 2013, ApJ , 764, 134
Lister, M. L., Aller, H. D., Aller, M. F., et al. 2009, AJ , 137, 3718
Murgia, M., Fanti, C., Fanti, R., et al. 1999, A&A, 345, 769
Nagai, H., Orienti, M., Kino, M., et al. 2012, MNRAS , 423, L122
Nagai, H., Suzuki, K., Asada, K., et al. 2010, PASJ , 62, L11
O'Dea, C. P., Dent, W. A., & Balonek, T. J. 1984, ApJ , 278, 89
Prandoni, I., & Seymour, N. 2015, Advancing Astrophysics with the Square Kilometre Array (AASKA14), 67
Suzuki, K., Nagai, H., Kino, M., et al. 2012, ApJ , 746, 140
Taylor, G. B., Gugliucci, N. E., Fabian, A. C., et al. 2006, MNRAS , 368, 1500
Walker, R. C., Dhawan, V., Romney, J. D., Kellermann, K. I., & Vermeulen, R. C. 2000, ApJ , 530, 233
Yamazaki, S., Fukazawa, Y., Sasada, M., et al. 2013, PASJ , 65, 30

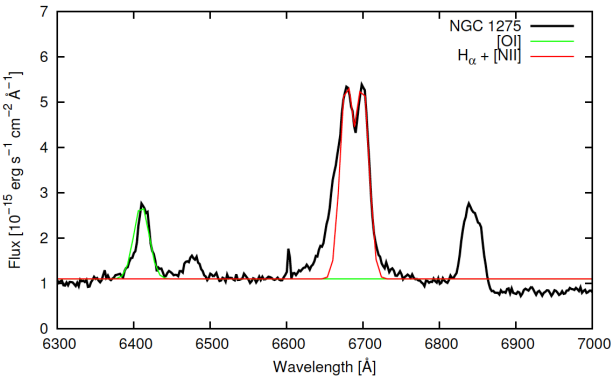

Fig. A1 Overall line spectra (the thick line) for the nucleus of NGC 1275 measured by HOWPol on the Kanata telescope. The [OI] flux (the line at $\sim$ 6400 Å) is scaled to the value reported in Ho et al. 1997. The sum of Hα (both broad and narrow) and [NII] lines are shown by the red line. We note that there is an ambiguity due to the unclear Hubble constant value adopted in Ho et al. 1997.

A The Hα line luminosity in NGC 1275

Here we evaluate the Hα luminosity ($L_{\rm H\alpha}$) of NGC 1275 using the observation data obtained by Kanata telescope's HOWPol (Hiroshima One-shot Wide-field Polarimeter) (Kawabata et al. 2008). We revisit the data used in Yamazaki et al. (2013) since (1) the flux was integrated over an aperture of $4''.7$ width, and (2) [NII] and narrow Hα lines were not taken into account, which may lead to an overestimate of $L_{\rm H\alpha}$. In Fig. A1 we show the optical spectrum at the nucleus of NGC 1275. The flux values of [OI] and narrow line of Hα are normalized to the literature values shown in Ho et al. (1997). The broad Hα and [NII] lines are adjusted to fit the observed data by eye inspection. Then we obtain that $L_{\rm H\alpha,broad} \sim 3.2 \times 10^{41}$ erg s^{-1}. Then we can derive the continuum luminosity

$$L_{5100} \sim 1 \times 10^{43} \ {\rm erg \ s^{-1}}, \tag{A1}$$

by using the well known empirical relation Greene and Ho (2005). Although there may include some contaminations from extended components (e.g., nebula, filaments etc), we use this value as a best estimate for $L_{\rm H\alpha}$. The obtained $L_{\rm H\alpha}$ is about three times smaller than that in Yamazaki et al. (2013).